Resonance neutron capture and transmission measurements and the stellar neutron capture cross sections of ^{134}Ba and ^{136}Ba

P. E. Koehler,[1] R. R. Spencer,[1] R. R. Winters,[2] K. H. Guber,[1] J. A. Harvey,[1] N. W. Hill,[1] and M. S. Smith[1]
[1]*Oak Ridge National Laboratory, Oak Ridge, Tennessee 37831-6354,*
[2]*Department of Physics, Denison University, Granville, Ohio 43023*
(Received 2 May 1996)

We have made high-resolution neutron capture and transmission measurements on isotopically enriched samples of ^{134}Ba and ^{136}Ba at the Oak Ridge Electron Linear Accelerator (ORELA) in the energy range from 20 eV to 500 keV. Previous measurements had a lower energy limit of 3–5 keV, which is too high to determine accurately the Maxwellian-averaged capture cross section at the low temperatures ($kT \approx 8-12$ keV) favored by the most recent stellar models of the *s* process. By fitting the data with a multilevel *R*-matrix code, we determined parameters for 86 resonances in ^{134}Ba below 11 keV and 92 resonances in ^{136}Ba below 35 keV. Astrophysical reaction rates were calculated using these parameters together with our cross section data for the unresolved resonance region. Our results for the astrophysical reaction rates are in good agreement with the most recent previous measurement at the classical *s*-process temperature $kT=30$ keV, but show significant differences at lower temperatures. We determined that these differences were due to the effect of resonances below the energy range of previous experiments and to the use of incorrect neutron widths in a previous resonance analysis. Our data show that the ratio of reaction rates for these two isotopes depends more strongly on temperature than previous measurements indicated. One result of this temperature dependence is that the mean *s*-process temperature we derived from a classical analysis of the branching at ^{134}Cs is too low to be consistent with the temperature derived from other branching points. This inconsistency is evidence for the need for more sophisticated models of the *s* process beyond the classical model. We used a reaction network code to explore the changes in the calculated isotopic abundances resulting from our new reaction rates for an *s*-process scenario based on a stellar model. These calculations indicate that the previously observed 20% discrepancy with respect to the solar barium abundance is reduced but not resolved by our new reaction rates. [S0556-2813(96)04609-2]

PACS number(s): 26.20.+f, 25.40.Lw, 27.60.+j, 97.10.Cv

I. INTRODUCTION

Recent calculations [1–3] of the nucleosynthesis occurring in the helium shell of low-mass red giant stars on the asymptotic branch have for the first time come reasonably close to reproducing the observed *s*-process isotopic abundances. However, exceptions to the general good agreement between the calculation and the data were observed for the isotopes ^{134}Ba and ^{136}Ba. These two nuclei are among the few so-called *s*-only isotopes because they are shielded against contributions to their abundances from the *r* process by stable isobars of xenon. Because their abundances are thought to arise almost exclusively from the *s* process, the *s*-only isotopes are the most important calibration points for the models; hence, the difference between the observed and calculated abundances for ^{134}Ba and ^{136}Ba may be a sign of a problem with the model. A major change in the models of Refs. [1–3] with respect to previous models of the *s* process in intermediate-mass stars [4], or in the so-called classical *s* process [5], is that the temperature at which most of the neutron exposure occurs is much lower, $kT \approx 8-12$ keV compared to $kT \approx 30$ keV. Because of the lower temperature, it seemed possible that the differences between the calculated and observed abundances for ^{134}Ba and ^{136}Ba observed in Refs. [1–3] were due to the use of incorrect Maxwellian-averaged neutron capture cross sections (commonly referred to as the ''reaction rates'') for these isotopes. To determine accurately the reaction rates needed for the nucleosynthesis calculations at these lower temperatures, it is necessary to measure the cross sections to energies as low as a few hundred eV. Most previous measurements had a lower-energy limit of about 3–5 keV. A dramatic illustration of the possible systematic errors inherent in extrapolating to lower energies was provided by recent measurements of the ^{138}Ba (n,γ) cross section [6]. Although good agreement was obtained with the older [7,8] reaction rate at $kT=30$ keV, the new results were 51% higher at $kT=10$ keV. Most of this discrepancy was due to the existence of strong resonances below the energy cutoff ($E_n > 3$ keV) of the older experiment. The major motivation of the present experiment was to measure the neutron capture cross sections for ^{134}Ba and ^{136}Ba at energies below the limit of the previous measurements [9,10] to ascertain the effect of possible low-energy resonances on the reaction rate at the lower temperatures favored by the new stellar models. Because of the wide energy range, excellent energy resolution, relatively high flux, well-shielded flight paths, and the capability for several simultaneous measurements on different flight paths, the Oak Ridge Electron Linear Accelerator (ORELA) facility is ideally suited for making these measurements.

A second problem with previous determinations of the reaction rates for these isotopes is the lack of high-quality neutron transmission data. Because the measurements were necessarily made with relatively thick samples, substantial

TABLE I. Sample details.

Sample	Thickness of Ba (10^{-3} atom/b)[b]	Weight of $BaCO_3$ (g)	Container weight[a] (g)
^{134}Ba, capture	1.135	3.711	0.489
^{136}Ba, capture	2.788	9.198	0.687
^{134}Ba, transmission	12.25	3.703	-
^{136}Ba, transmission	12.65	9.368	-

[a]Total weight of aluminum plus glue.

[b]In this notation, the ''thickness'' of the sample is defined as its mass (in units of the number of barium atoms) divided by its area (in barns) perpendicular to the direction of the neutron beam.

corrections for resonance self-shielding and multiple scattering had to be applied to the data. The size of these corrections scales with the ratio of the statistical factor times the neutron width to the total width, $g_J\Gamma_n/\Gamma$. In the unresolved region, corrections for these effects can be calculated accurately using average resonance parameters. However, the size of the corrections varies considerably from one resonance to the next; hence, in the resolved resonance region precise knowledge of the neutron widths is needed to calculate these corrections accurately. The second major motivation for the present work was to make high-quality transmission measurements to reduce substantially the systematic uncertainties associated with these corrections. Another reason for making the transmission measurements has to do with the fact that theoretical calculations using nuclear models must still be relied upon to obtain the reaction rates for many important radioactive branching points in the *s* process path (e.g., ^{134}Cs). The accuracy with which these models can calculate the required reaction rates needs to be improved. For example, global statistical model calculations [11,12] are typically accurate to about a factor of 2. Model calculations constrained to reproduce measured cross sections for nuclei near branching points may be accurate to approximately 20% [13]. The models may be improved by providing more and better input data with which to constrain them. Because we analyzed both capture and transmission measurements at the same time, the resulting resonance parameters are more complete than those obtained from the analysis of only one or the other of these sets of data. The resonance parameters, and average properties calculated from them, should provide valuable input for improving the nuclear models.

A final motivation for the present work was to compare capture cross sections which we measured using the pulse height weighting technique to recent measurements made with a 4π BaF_2 detector [9,14]. Problems with previous measurements made using the pulse height weighting technique have called into question the accuracy of the technique. The problems are thought to be greatest for samples having relatively hard capture γ-ray spectra as might be expected for nuclei near closed neutron shells such as the barium isotopes studied herein. Considerable effort has been devoted to understanding past problems and in obtaining accurate weighting functions. The result is that it is now believed [15–17] that accurate weighting functions can be calculated and that past problems have been resolved. A comparison of our data to those measured with the 4π BaF_2 detector should serve as a further test of the accuracy of our weighting functions.

II. EXPERIMENTAL PROCEDURES

The measurements were performed using the ORELA white neutron source facility. The ORELA was operated at a pulse rate of 530 Hz, a pulse width of 7 ns, and a power of approximately 4–7 kW during the course of two 3-week runs. During the first run, capture data were taken on ^{134}Ba while transmission measurements were made on ^{136}Ba. This arrangement was switched for the second run. The dimensions of the samples and their holders were changed between runs to meet the different needs of the capture and transmission experiments.

The samples were in the form of isotopically enriched, compressed barium carbonate powder. Details of the samples are given in Tables I and II. Our capture samples were thinner than those used in previous measurements [9,10]; hence, the often substantial resonance self-shielding corrections were smaller than in these previous works. The ^{134}Ba powder was loaned to us by the Forschungszentrum Karlsruhe. The ^{136}Ba powder was rented from the Oak Ridge Enriched Stable Isotope Pool. Approximately half of the ^{134}Ba sample had to be converted from nitrate to carbonate. The conversion was carried out by scientists in the Analytical Chemistry Division at Oak Ridge National Laboratory. To ensure precise $BaCO_3$ stoichiometry, the powders were heated to 800 C in a CO_2 atmosphere for approximately 1 h [18]. No significant change in weight was observed as a result of the heating. The samples for the capture measurements were compressed in a die into two disks 2.54 cm in diameter. The disks were encapsulated in thin-walled aluminum cans and mounted one above the other in the vacuum of the beam line between the detectors. The samples for the transmission measurements were compressed by hand into copper holders with thin aluminum windows.

The transmission measurements were made on ORELA

TABLE II. Isotopic compositions of samples.

Sample	Atomic percent						
	^{130}Ba	^{132}Ba	^{134}Ba	^{135}Ba	^{136}Ba	^{137}Ba	^{138}Ba
^{134}Ba	<0.1	<0.1	84.20	3.87	1.88	1.79	8.23
^{136}Ba	<0.02	<0.02	0.08	0.96	92.92	1.73	4.31

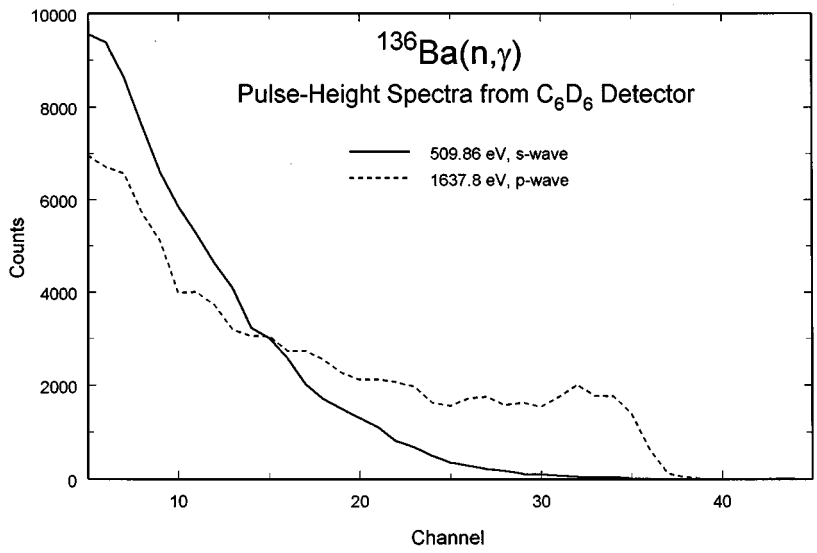

FIG. 1. Representative pulse height spectra for an *s*-wave (solid curve) and a *p*-wave (dashed curve) resonance in ^{136}Ba. The off-resonance background has been subtracted and the data for the *p*-wave resonance have been normalized (by a factor of 4.06) so that the spectra have equal areas.

flight path 1 with a source-to-detector distance of 79.759 m. The neutron detector was a ^{6}Li loaded glass scintillator. A ^{10}B filter was used to remove overlap neutrons from preceding beam bursts, and a 0.64 cm thick Pb filter was used to reduce effects due to the γ flash at the beginning of each pulse. The $BaCO_3$ sample was exchanged periodically with an empty container having the same dimensions as the sample holder and with polyethylene and bismuth absorbers which were used for determination of backgrounds. The cycle through the four samples took about 1 h under normal beam conditions. Further details of the transmission apparatus can be found in Ref. [19].

The capture measurements were made on ORELA flight path 7 at a source-to-sample distance of 40.12 m. A ^{10}B filter was used to remove overlap neutrons from preceding beam bursts and a 1.27 cm thick lead filter was used to reduce γ-flash effects. The capture apparatus has been improved in several significant ways compared to the setup [20] used in many of the previous ORELA measurements. First, the C_6F_6 detectors have been replaced by C_6D_6. Second, the fairly massive vacuum beam line near the detectors has been replaced by a low-mass graphite fiber tube. Third, the sample holder was significantly reduced in mass. These changes were made to lower the neutron sensitivity of the detection apparatus by reducing the number of γ rays produced by neutrons scattered from the sample and to make the calculation of the pulse height weighting functions simpler and more reliable. Fourth, the pulse height weighting functions, which are used to make the detector efficiency independent of the details of the capture γ-ray cascade, have been improved in two important ways. The first change has been to acquire both pulse height and time-of-flight data so that the weighting functions could be applied off line. This allows the weighting functions to be changed during the analysis if necessary. The second change has been to calculate the weighting functions more accurately by using the code EGS4 [21]. The calculation includes the details of the sample, the detectors, and the beam line in their vicinity. It has been shown [16] that these calculations can reproduce the measured pulse height spectra for resonances with known γ-ray cascades, lending confidence that the weighting functions are calculated accurately. The representative pulse height spectra for both an *s*- and a *p*-wave resonance in ^{136}Ba shown in Fig. 1 illustrate that the shape of the spectra can change substantially; hence, the effect of the weighting functions can be significant.

A ^{6}Li loaded glass scintillator [20], located 43 cm ahead of the sample in the neutron beam, was used to measure the energy dependence of the neutron flux. Separate sample-out background measurements were made using aluminum cans of the same dimensions as the sample holder. In addition, measurements made with a carbon sample were used, after proper normalization to the number of sample atoms times the average cross section, to subtract the smoothly varying background due to sample scattered neutrons. The overall normalization of the counts to cross section was made via the saturated resonance technique [22] using the 4.9 eV resonance in the ^{197}Au(n,γ) cross section.

In the unresolved resonance region (above 11 keV in ^{134}Ba and 35 keV in ^{136}Ba), the relatively small corrections for multiple scattering and resonance self-shielding were calculated using the code SESH [23] and applied to the data. The overall correction factor for these effects was about 0.99 for ^{134}Ba and 0.97 for ^{136}Ba. The data in this region were also corrected for the isotopic impurities in the samples using the cross sections of Refs. [9] and [6]. To make this correction, we extrapolated the data of Refs. [9] (for ^{135,137}Ba) and [6] (for ^{138}Ba) to 500 keV using the calculated cross sections of Ref. [11] after the calculations had been normalized to the data in the 50–100 keV region. The correction factor (to convert from the cross section for the entire sample to the cross section for the major isotope only) for isotopic impurities was about 1.06 for ^{134}Ba and 0.96 for ^{136}Ba.

III. RESONANCE ANALYSIS AND RESULTS

The multilevel *R*-matrix code SAMMY [24] was used to fit the capture and transmission data. A radius of 5.14 fm was used for both *s* and *p* waves for both isotopes. Unless the resonance is strong in both the transmission and capture data, there is some arbitrariness in the resonance parameters obtained from the fits to the data. With the aim of obtaining the most meaningful set of parameters, we attempted to mini-

TABLE III. ^{134}Ba resonance parameters.

	E_n (keV)	l	$g\Gamma_n$ (meV)	Γ_γ (meV)	$\frac{g\Gamma_n\Gamma_\gamma}{\Gamma}$ (meV)
1	0.1020	0	161.87 ±0.54	65.13 ±0.10	46.44 ±0.40
2	0.3276	(0)	2.09 ±0.09	77	2.03 ±0.10
3	0.3742	(0)	6.16 ±0.16	77	5.70 ±0.14
4	0.4990	0	50.91 ±0.80	65.6 ±1.8	28.66 ±0.42
5	0.8125	(0)	9.10 ±0.32	77	8.14 ±0.25
6	0.970	0	68.5 ±1.3	77.4 ±2.7	36.34 ±0.69
7	1.1090	(0)	11.07 ±0.51	77	9.68 ±0.39
8	1.2213	0	818.8 ±7.8	58.0 ±1.0	54.16 ±0.86
9	1.4570	(1)	26.0 ±1.0	73	19.17 ±0.57
10	1.5165	(1)	11.80 ±0.60	73	10.92 ±0.52
11	1.5929	(1)	17.00 ±0.10	73	13.79 ±0.06
12	1.6165	0	288.3 ±6.3	69.1 ±4.3	55.7 ±2.8
13	1.7035	(1)	22.6 ±1.0	73	19.57 ±0.71
14	1.8853	0	607 ±11	64.2 ±1.6	58.1 ±1.3
15	2.0020	(1)	7.18 ±0.53	73	6.54 ±0.45
16	2.0750	(1)	6.82 ±0.52	73	6.24 ±0.44
17	2.2112	(1)	20.0 ±1.0	73	15.70 ±0.67
18	2.2930	(1)	5.64 ±0.44	73	5.43 ±0.41
19	2.4670	(1)	8.51 ±0.70	73	7.62 ±0.57
20	2.6479	(1)	2.28 ±0.22	73	2.21 ±0.21
21	2.6593	0	3158±30	62.8 ±2.1	61.6 ±2.0
22	2.8540	0	1580±26	62.3 ±2.0	59.9 ±1.9
23	2.9572	(1)	18.3 ±1.2	73	16.26 ±0.98
24	3.1376	(1)	87.4 ±2.3	73.5 ±5.5	39.9 ±1.6
25	3.2286	1	246±11	59.1 ±4.8	47.7 ±3.2
26	3.2536	(1)	55.7 ±5.1	89 ±15	34.2 ±1.7
27	3.4176	0	1531±31	73.9 ±2.6	70.5 ±2.4
28	3.6829	(1)	33.2 ±3.4	73	22.8 ±1.7
29	3.8557	1	422±18	67.6 ±2.8	58.3 ±2.1
30	3.9005	0	6865±64	56.7 ±2.9	56.2 ±2.8
31	3.9367	(1)	46.0 ±3.2	73	35.0 ±2.2
32	4.0010	(1)	20.3 ±2.2	73	17.8 ±1.7
33	4.1380	0	2695±47	72.2 ±3.0	70.3 ±2.8
34	4.2890	0	811±29	70.1 ±2.9	64.5 ±2.5
35	4.4982	(1)	31.2 ±3.0	73	25.7 ±2.1
36	4.5844	0	9325±85	65.6 ±4.5	65.1 ±4.4
37	4.8358	(1)	154.2 ±8.0	115 ±12	92.3 ±3.3
38	4.8639	0	2108±52	56.6 ±3.6	55.1 ±3.4
39	4.9440	(1)	23.2 ±3.0	73	20.0 ±2.3
40	4.9730	(1)	80.5 ±6.4	73	51.9 ±2.9
41	5.3200	0	4141±75	188.7 ±6.2	180.5 ±5.7
42	5.3599	1	286±27	93.2 ±6.8	70.3 ±4.2
43	5.3857	(0)	122 ±16	97±12	54.0 ±3.1
44	5.4264	(1)	105 ±13	119 ±16	55.8 ±2.9
45	5.9336	(1)	82.4 ±1.8	64.6 ±9.6	50.3 ±3.0
46	6.0404	0	994±49	89.0 ±5.0	81.7 ±4.2
47	6.1260	(1)	22.0 ±3.2	73	19.1 ±2.5
48	6.1759	(1)	58.4 ±4.4	73	41.7 ±2.4
49	6.2064	1	1304 ±60	67.8 ±4.4	64.4 ±4.0
50	6.3010	0	7580 ±120	77 ±18	76 ±17
51	6.5280	(1)	71.5 ±7.8	73	48.0 ±3.8
52	6.6049	(1)	166 ±26	86.1 ±9.3	56.7 ±3.7
53	6.7669	(1)	169 ±28	72.7 ±8.0	50.8 ±4.7
54	6.8593	(1)	86 ±16	62.3 ±9.4	36.1 ±3.2
55	7.0310	(1)	61.0 ±9.1	81 ±14	34.8 ±3.2
56	7.0719	(1)	19.4 ±1.8	73	17.1 ±1.4
57	7.1906	1	408 ±47	76.1 ±5.2	64.1 ±3.9
58	7.5340	(1)	42.8 ±3.6	73	33.1 ±2.2
59	7.6205	0	1313±78	79.9 ±4.9	75.3 ±4.4
60	7.7370	(1)	43.6 ±3.6	73	33.6 ±2.2
61	8.1412	(1)	224 ±44	83.5 ±6.8	60.8 ±4.8
62	8.1543	(1)	568±63	95.0 ±6.5	81.4 ±4.9
63	8.2116	0	12470.00 ±200	85.7 ±5.8	85.1 ±5.7
64	8.3427	(1)	93 ±13	86 ±15	60.4 ±5.4
65	8.3740	(1)	159 ±28	109 ±15	64.7 ±5.1
66	8.7531	(1)	66±11	79 ±14	36.0 ±3.8
67	8.8370	(1)	553 ±68	98.6 ±5.6	145.4 ±7.7
68	8.9484	(1)	33.6 ±3.0	73	27.3 ±2.1
69	9.0659	(1)	420±64	101.7 ±5.9	137.0 ±8.7
70	9.1400	(1)	67.2 ±1.0	73	46.0 ±2.4
71	9.1600	(1)	283 ±52	65.5 ±4.8	89.5 ±6.9
72	9.2757	0	26880 ±330	102.7 ±8.8	102.3 ±8.7
73	9.3550	(1)	346 ±58	105 ±12	131.0 ±7.2
74	9.4106	(1)	72.2 ±5.0	73	48.3 ±2.4
75	9.6494	0	5570 ±180	66.4 ±5.8	65.6 ±5.7
76	9.7322	0	10570 ±230	93.6 ±6.7	92.8 ±6.6
77	9.7600	(1)	185 ±27	95 ±14	93.7 ±6.6
78	9.8763	(1)	381 ±68	110 ±13	139.5 ±8.1
79	10.0166	(1)	146 ±19	97 ±15	83.3 ±6.3
80	10.0782	(1)	2340 ±150	76.1 ±4.3	143.0 ±7.6
81	10.0968	(0)	1590 ±130	69.9 ±5.6	67.0 ±5.1
82	10.1221	(1)	418±74	50.9 ±3.9	81.9 ±5.8
83	10.2061	(1)	395 ±80	90.1 ±6.5	124 ±10
84	10.4820	0	25130 ±390	76.1 ±6.5	75.9 ±6.5
85	10.5102	(1)	230 ±41	79 ±12	93.7 ±7.6
86	10.5963	(1)	143 ±20	91 ±15	80.1 ±6.6

mize the arbitrariness by employing the procedures outlined below.

For some resonances, firm spin (s- or p-wave) assignments could be made based on the shape of the resonance in the transmission data. Furthermore, for ^{136}Ba, it has been suggested that p-wave resonances should have a more energetic (i.e., ''harder'') γ-ray spectrum than s-wave ones [10]. We were able to confirm this expectation. In our data, resonances with a clear s-wave shape in the transmission spectrum almost always had a much softer γ-ray spectrum than those with a clear p-wave shape. For some resonances without a clear s- or p-wave shape in the transmission data, we were sometimes able to use the γ-ray spectra, such as those shown in Fig. 1, to make a tentative l-value assignment. Also, the average p-wave radiation width for the 18 firm p-wave assignments in ^{136} Ba was more than twice as large as the average for the 18 firm s-wave resonances. We used this information to make a tentative l-value assignment in several cases where an assignment was not otherwise possible.

TABLE IV. ^{136}Ba resonance parameters.

	E_n (keV)	l	$g\Gamma_n$ (meV)	Γ_γ (meV)	$\frac{g\Gamma_n\Gamma_\gamma}{\Gamma}$ (meV)
1	0.4477	(0)	3.27 ± 0.22	87	3.15 ± 0.20
2	0.5099	0	160.0 ± 4.7	63.5 ± 0.6	45.46 ± 0.49
3	0.5240	(0)	3.69 ± 0.26	87	3.54 ± 0.24
4	1.6378	1	91.5 ± 3.2	272.0 ± 13	68.5 ± 2.0
5	2.1391	0	661 ± 18	84.0 ± 1.4	74.5 ± 1.1
6	2.2988	0	1334 ± 26	62.2 ± 1.1	59.4 ± 1.0
7	2.8267	1	169.0 ± 8.5	252.5 ± 14	126.6 ± 5.1
8	3.4114	1	82.0 ± 4.6	196	67.8 ± 3.2
9	3.4550	0	6762 ± 64	45 ± 10	45 ± 10
10	3.5447	(0)	51.0 ± 8.6	60 ± 14	27.6 ± 1.0
11	4.3157	0	478 ± 21	59.3 ± 1.7	52.8 ± 1.4
12	4.7019	1	1703 ± 34	192.4 ± 3.2	313.9 ± 4.4
13	4.9476	1	182 ± 19	149.0 ± 8.0	113.0 ± 7.7
14	6.1257	0	11620 ± 130	80.7 ± 3.3	80.1 ± 3.2
15	6.1657	(1)	393 ± 17	160.3 ± 6.7	113.9 ± 3.7
16	6.6418	(1)	89.5 ± 4.7	196	61.4 ± 2.2
17	7.0436	(1)	62.5 ± 4.5	196	47.4 ± 2.6
18	7.2374	0	126220 ± 510	160 ± 50	160 ± 50
19	7.5524	1	2075 ± 59	182.2 ± 5.2	167.5 ± 4.4
20	7.7473	(1)	37.6 ± 2.8	196	31.5 ± 2.0
21	8.8015	1	166 ± 10	150 ± 13	106.9 ± 3.4
22	8.9106	1	899 ± 43	196.3 ± 6.7	161.1 ± 4.7
23	9.1759	(1)	22.6 ± 2.3	196	20.3 ± 1.8
24	9.9650	0	14160 ± 260	87.2 ± 4.8	86.7 ± 4.7
25	10.1829	(1)	966 ± 55	140.0 ± 5.9	122.3 ± 4.6
26	10.2528	1	829 ± 46	137.8 ± 5.8	206.8 ± 7.1
27	10.4446	(1)	204 ± 18	131.1 ± 9.4	79.8 ± 3.3
28	11.0278	(1)	72.0 ± 6.7	196	52.7 ± 3.6
29	11.1551	0	2030 ± 150	58.9 ± 3.4	57.2 ± 3.2
30	11.7696	0	8610 ± 260	62.2 ± 4.1	61.8 ± 4.0
31	12.2975	(1)	36.9 ± 5.6	196	31.0 ± 4.0
32	12.8876	(1)	574 ± 80	191 ± 18	143 ± 11
33	13.1550	(1)	808 ± 84	121.4 ± 7.6	105.5 ± 5.9
34	13.3179	(1)	1098 ± 82	128.4 ± 8.1	208 ± 11
35	13.7672	0	25640 ± 550	94.7 ± 8.6	94.4 ± 8.5
36	13.8622	(1)	19.6 ± 4.6	196	17.8 ± 3.8
37	14.5517	1	2130 ± 120	226 ± 10	373 ± 14
38	15.1816	0	10850 ± 420	92.0 ± 7.1	91.2 ± 7.0
39	15.6127	(1)	146 ± 19	196	106 ± 10
40	16.0480	(1)	17.1 ± 3.7	196	15.7 ± 3.1
41	16.1453	(0)	1280 ± 120	89.5 ± 8.2	83.7 ± 7.2
42	16.2355	(1)	79.2 ± 9.8	196	65.9 ± 6.8
43	16.9832	(0)	1200 ± 260	81.0 ± 7.3	75.9 ± 6.5
44	17.0673	(1)	1650 ± 150	122.8 ± 6.7	214 ± 10
45	17.3050	(1)	513 ± 49	168 ± 10	126.6 ± 5.6
46	17.9286	0	8500 ± 500	84.6 ± 6.1	83.8 ± 6.0
47	18.0381	(1)	260 ± 26	125 ± 12	127.4 ± 8.0
48	18.4908	(1)	2090 ± 180	123.2 ± 5.8	220.4 ± 9.5
49	18.6722	(1)	83 ± 11	196	68.5 ± 7.5
50	18.8980	(0)	3210 ± 200	104.0 ± 6.7	100.7 ± 6.3
51	19.2121	(1)	300 ± 30	100 ± 10	120.0 ± 8.6
52	19.7783	1	7320 ± 280	249.5 ± 9.0	467 ± 16
53	19.9266	(0)	3240 ± 410	61.4 ± 4.9	60.3 ± 4.7
54	20.3386	(1)	86 ± 12	196	70.5 ± 8.0
55	20.3978	(1)	522 ± 48	132.8 ± 9.1	176.0 ± 8.0
56	20.8125	(1)	77 ± 12	196	64.4 ± 8.4
57	21.3491	(1)	1406 ± 140	132.0 ± 8.6	120.7± 7.2
58	21.4527	(1)	87 ± 9.7	196	71.2 ± 6.5
59	21.5944	1	7220 ± 330	171.0 ± 9.5	167.0 ± 9.1
60	22.0810	0	2170 ± 500	59.4 ± 9.8	57.8 ± 9.3
61	22.2493	1	3780 ± 290	123.3 ± 7.7	231 ± 14
62	22.2954	(1)	690 ± 200	208 ± 24	160 ± 12
63	22.6238	(1)	900 ± 260	141 ± 14	121.9 ± 9.9
64	22.9630	(1)	30.0 ± 6.7	196	26.0 ± 5.0
65	23.2763	(1)	126 ± 17	196	95.4 ± 9.7
66	24.1486	0	26000 ± 1200	138 ± 15	137 ± 15
67	24.2773	(1)	640 ± 170	140 ± 24	195 ± 21
68	24.7086	(1)	60 ± 12	196	46.0 ± 7.0
69	24.7932	(1)	3200 ± 300	146 ± 14	140 ± 13
70	25.2647	1	8290 ± 440	199 ± 15	194 ± 14
71	25.8246	0	6460 ± 850	80 ± 11	79 ± 11
72	26.7256	(1)	243 ± 73	148 ± 44	92 ± 20
73	27.2784	1	3950 ± 450	192 ± 11	350 ± 19
74	27.5759	(0)	5130 ± 980	108 ± 15	106 ± 14
75	27.7934	(1)	2470 ± 340	141 ± 14	253 ± 23
76	28.4487	(1)	480 ± 130	126 ± 37	165 ± 35
77	28.6100	(0)	1220 ± 360	74 ± 21	70 ± 19
78	28.9149	1	3210 ± 450	220 ± 13	387 ± 21
79	29.3066	(1)	2520 ± 420	141 ± 11	254 ± 18
80	29.6170	0	17900 ± 1500	108 ± 16	107 ± 16
81	29.6880	(1)	1010 ± 300	108 ± 16	178 ± 24
82	30.3440	(1)	6160 ± 910	137 ± 10	262 ± 18
83	31.3100	1	760 ± 190	293 ± 78	331 ± 56
84	32.3622	1	7950 ± 730	129 ± 12	250 ± 22
85	32.8318	(0)	4600 ± 1100	86 ± 16	84 ± 15
86	32.9031	(1)	4440 ± 570	200 ± 16	367 ± 27
87	33.2076	0	9100 ± 1500	86 ± 16	85 ± 16
88	33.5434	(1)	1000 ± 300	137 ± 38	120 ± 30
89	33.6335	(1)	4710 ± 690	125 ± 12	237 ± 22
90	33.9280	(1)	192 ± 42	196	129 ± 19
91	34.2683	(1)	13030 ± 970	158 ± 13	308 ± 25
92	34.5552	(1)	1430 ± 420	191 ± 28	168 ± 22

The following procedures were used to obtain the resonance partial widths from the data. For resonances which were observed as strong dips in the transmission spectra, Γ_n and $\Delta\Gamma_n$ were determined by fitting the transmission spectrum by initially fixing Γ_γ to the average value given in Ref. [25]. The Γ_n obtained was then held constant while the capture data were fitted to obtain Γ_γ and $\Delta\Gamma_\gamma$. The new Γ_γ was then used to recalculate the transmission. For most of these resonances, $\Gamma_n \gg \Gamma_\gamma$, and so there was little sensitivity in the transmission data to variations in Γ_γ and vice versa (except that the capture area depends on the Γ_n value through its influence on the self-shielding and multiple scattering corrections). Hence, the new Γ_γ did not affect the fit to the transmission data noticeably. The few strong resonances

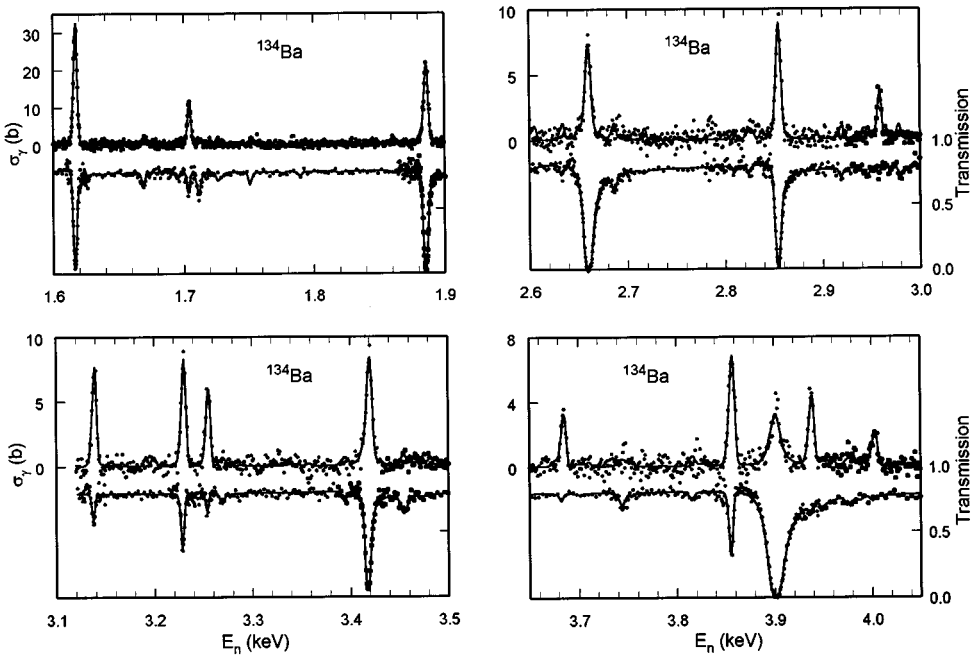

FIG. 2. Representative data (points) and SAMMY fits (solid curves) from our capture (top) and transmission (bottom) measurements on ^{134}Ba. The effective capture cross sections have not been corrected for finite-thickness sample effects. The corrections are calculated by the code SAMMY; hence, the fits represent the theoretical cross sections, calculated from the resonance parameters, after adjustment for these sample-dependent effects. The scales for the capture data are on the left of each plot whereas the transmission scales are on the right. The transmission data between resonances or over broad resonances were sometimes averaged over several energies to reduce the statistical fluctuations. Several of the resonances in the energy region below the previous experiments [9,10] are shown.

at low energies having $\Gamma_n \approx \Gamma_\gamma$ were fitted using the same procedure because the calculated transmission was still most sensitive to Γ_n and the capture to Γ_γ. In the above cases the uncertainties in Γ_n and Γ_γ were assumed to be uncorrelated when calculating the uncertainty associated with the capture kernel, $g_J\Gamma_n\Gamma_\gamma/\Gamma$. Almost all of these strong resonances could be assigned a firm l value on the basis of their shape in the transmission spectra. These resonances with firm l-value assignments were used to recalculate the average s- and p-wave radiation widths, $\langle\Gamma_{\gamma l}\rangle$. For ^{134}Ba, we obtained $\langle\Gamma_{\gamma 0}\rangle = 77$ meV and $\langle\Gamma_{\gamma 1}\rangle = 73$ meV. For ^{136}Ba, we obtained $\langle\Gamma_{\gamma 0}\} = 87$ meV and $\langle\Gamma_{\gamma 1}\rangle = 196$ meV.

Resonances which were visible, but not strong, in the transmission spectra were fitted initially by allowing

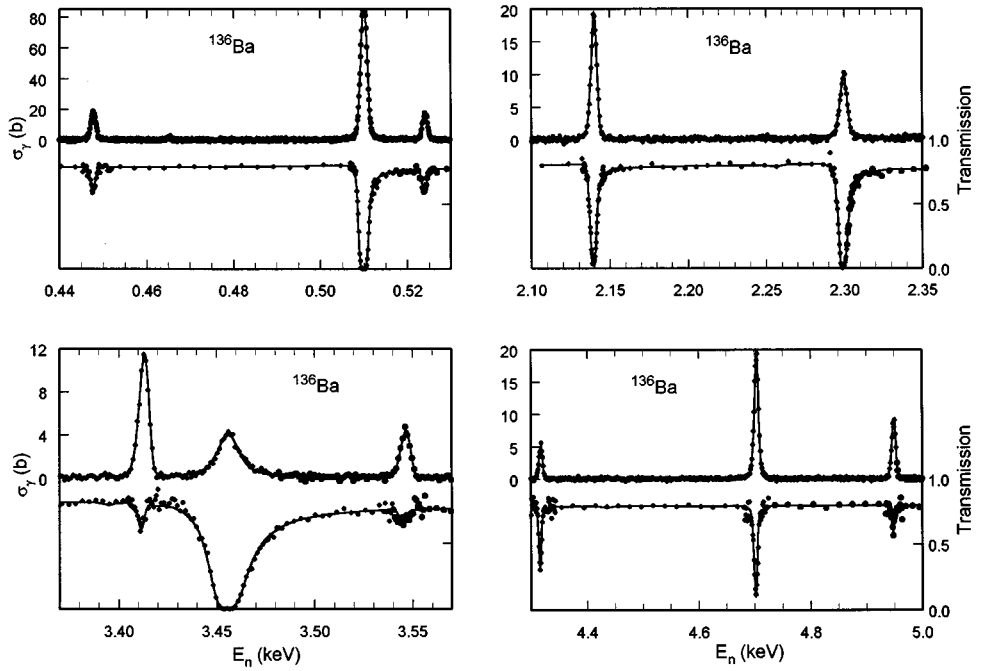

FIG. 3. Representative data (points) and SAMMY fits (solid curves) from our capture and transmission measurements on ^{136}Ba. See the caption of Fig. 2 for details.

TABLE V. Average resonance properties.

Isotope	Property	Present Work	Ref. [10]	Ref. [25]
^{134}Ba	$\langle\Gamma_{\gamma 0}\rangle$	77.8 ± 4.8 [a] ± 26 [b] meV	120 ± 20 meV	120 ±20 meV
	D_0	371 ± 36 eV	127 ± 10 eV [c]	D = 127 ± 10 eV
	$10^4 S_0$	1.4 ± 0.4	0.85 ± 0.3	0.53 ± 0.14
	$\langle\Gamma_{\gamma 1}\rangle$	85.1 ± 9.4 [a] ± 17 [b] meV	-	-
	D_1	163 ± 11 eV	-	-
	$10^4 S_1$	3.2 ± 0.6	≈0.8	0.8 ± 0.3
^{136}Ba	$\langle\Gamma_{\gamma 0}\rangle$	86 ± 10 [a] ± 24 [b] meV	125 ± 30 [b] meV	125 ± 30 meV
	D_0	1213 ± 119 eV	750 - 1200 eV	430 ± 35 eV
	$10^4 S_0$	0.86 ± 0.23	''close to other Ba isotopes''	0.8 ± 0.3
	$\langle\Gamma_{\gamma 1}\rangle$	163 ± 15 [a] ± 45 [b] meV	''considerably larger than for *s*-wave''	-
	D_1	522 ± 34 eV	-	-
	$10^4 S_1$	1.8 ± 0.3	-	-

[a]Uncertainty calculated by propagating the individual uncertainties.
[b]Standard deviation of the distribution of radiation widths.
[c]Calculated assuming all resonances below 5 keV are *s* wave.

Γ_n only to vary and holding Γ_γ fixed to the appropriate one of the average values given above. If the fit resulted in $\Gamma_n < 1/2\Gamma_\gamma$, then the capture data were also fitted in the same manner starting with the Γ_n value obtained from transmission. The somewhat arbitrary choice of $\Gamma_n < 1/2\Gamma_\gamma$ was made because it was found that there was very little sensitivity in the fit to the capture data to variations in Γ_γ when Γ_n was this small. The Γ_n values obtained from fitting the capture data were used to recalculate the transmission and checked versus the data. In all cases the Γ_n values obtained from the fits to the capture data were found to be consistent with the transmission data. Also, the uncertainties $\Delta\Gamma_n$ obtained from fitting the capture data were smaller than those obtained from fitting the transmission data for these resonances. For resonances where the initial fit to the transmission data indicated that $\Gamma_n > 1/2\Gamma_\gamma$, the capture data were fitted, starting from the parameters obtained in the fit to the transmission, by letting both widths vary simultaneously. In these cases the correlation between the two widths was included in the calculation of the uncertainty in the capture kernel. The transmission was recalculated with the parameters obtained from the fit to the capture data. In all but one case, the calculated transmission was still consistent with the data. In this case (the 6.767 keV resonance in ^{134}Ba) the starting and fitted capture calculations were almost indistinguishable, but the fitted Γ_n was too small to be consistent with the transmission data. So we refitted the capture data while holding Γ_n fixed to the value obtained from the fit to the transmission. In this way good fits to both sets of data were obtained.

Finally, for resonances which were visible in the capture but not in the transmission data, an initial fit to the capture data was made while holding Γ_γ fixed to the appropriate average value. The capture data were either refitted while letting both widths vary or not refitted, depending on whether the fitted Γ_n was greater than or less than $1/2\Gamma_\gamma$ in a procedure similar to that described above. If both parameters were allowed to vary, then the correlation between them was taken into account while calculating the uncertainty in the capture kernel.

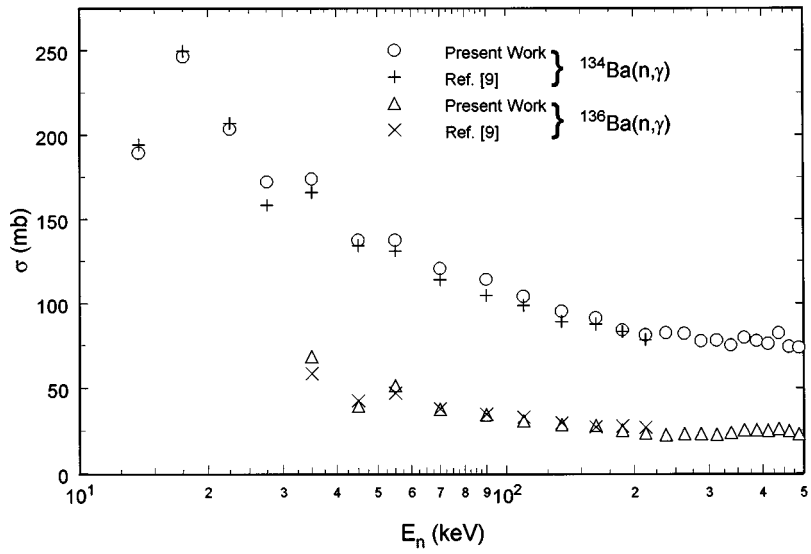

FIG. 4. Cross sections for the unresolved resonance region from our measurements (circles and triangles) and those of Ref. [9] (+'s and ×'s). Our data have been binned over the same energy intervals used in Ref. [9] for energies below 225 keV and in 25 keV wide bins to 500 keV.

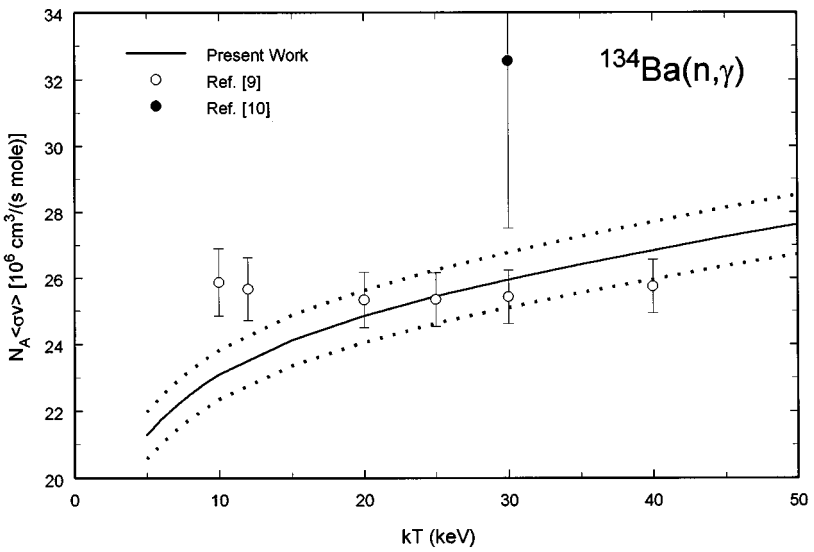

FIG. 5. The astrophysical reactivity for the ^{134}Ba(n,γ) reaction, calculated from our data (solid curve, with the dotted curves depicting the uncertainties), Ref. [9] (open circles), and Ref. [10] (solid circle).

The 7.237 keV resonance in ^{136}Ba needed special treatment. Because of the relatively large width of this resonance, multiple scattering effects are sizable even for the thin samples used in our capture measurement, and the single scattering correction in the code SAMMY was inadequate (SAMMY has been updated since the time of our analysis and the single scattering correction has been substantially improved). Therefore, we used the code FANAC [26] to calculate the multiple scattering correction for this resonance. The FANAC results indicated that about 50% of the measured capture area was due to multiple scattering. We also used FANAC to verify that the multiple scattering correction was negligible for all other resonances.

The resulting parameters are given in Tables III and IV. Example plots of the data and the fits are shown in Figs. 2 and 3. For ^{134}Ba we fitted 86 resonances between approximately 100 eV and 11 keV. Because the level spacing in ^{136}Ba is considerably larger than in ^{134}Ba, we were able to extend the resonance analysis to higher energies for this nucleus. For ^{136}Ba we fitted 92 resonances between 447 eV and 35 keV. The capture kernels $g_J\Gamma_n\Gamma_\gamma/\Gamma$, calculated from the resonance parameters, are also given in Tables III and IV.

For the few resonances which have $\Gamma_\gamma > \Gamma_n$ or $\Gamma_\gamma \approx \Gamma_n$, and where the resonance appears as a sufficiently strong dip in the transmission measurements, it is possible to obtain a relatively good measure of the capture kernel from the transmission measurements alone. We used this fact to check the capture kernels obtained from the analysis of both sets of data. Any differences might indicate, for example, problems with the pulse height weighting functions. In all cases we analyzed, the capture kernels obtained by the two methods were consistent within the experimental uncertainties.

We did not apply any corrections to the capture kernels to account for the background caused by the prompt detection of neutrons scattered by the sample. With the changes that have been made to our apparatus over the past few years, this correction should be negligible for all the resonances measured herein with the possible exception of the 7.237 keV resonance in ^{136}Ba. We can estimate the size of the correction by using the recent results from measurements of the ^{208}Pb(n,γ) cross section made with an apparatus similar to ours at Geel [27]. In Ref. [27] it was estimated that 1/3 of the measured area of the 77.85 keV resonance was due to the

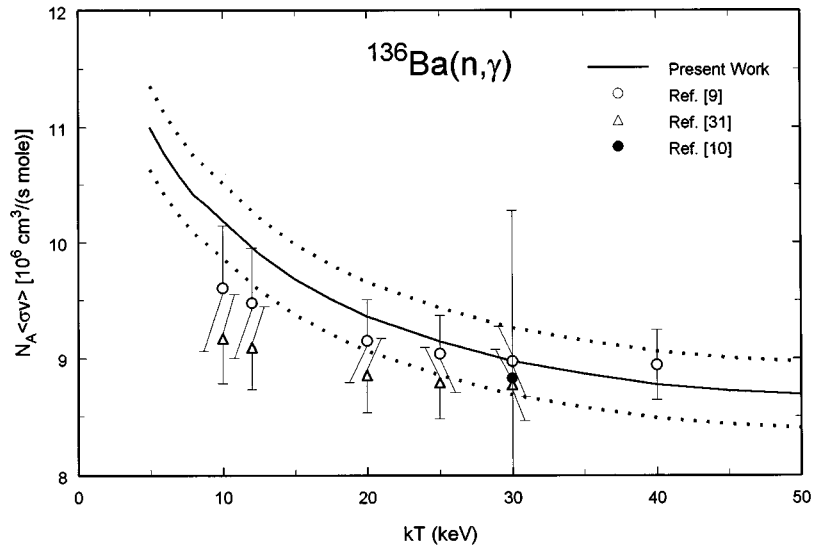

FIG. 6. The astrophysical reactivity for the ^{136}Ba(n,γ) reaction, calculated from our data (solid curve, with the dotted curves depicting the uncertainties), Ref. [9], (open circles), Ref. [10] (solid circle), and Ref. [31] (open triangles).

TABLE VI. Maxwellian averaged neutron capture cross sections.

Thermal energy kT (keV)	$\langle \sigma v \rangle / v_T$ (mb) ^{134}Ba	^{136}Ba
5.0	360.0 ± 12	186.0 ± 6.1
8.0	301.0 ± 9.7	139.4 ± 4.5
10.0	276.0 ± 8.8	122.0 ± 3.9
15.0	236.0 ± 7.4	94.6 ± 3.0
20.0	210.3 ± 6.7	79.2 ± 2.5
25.0	192.3 ± 6.1	69.2 ± 2.2
30.0	179.0 ± 5.7	62.0 ± 2.0

prompt capture of scattered neutrons and that $\Gamma_n = 958$ eV and $\Gamma_\gamma = 125$ meV. Assuming that $A_m = A_t\,(1 + C\Gamma_n)$, where A_m and A_t are the measured and true capture areas, respectively, it follows that the correction factor is $C = 5.22 \times 10^{-7}$ meV^{-1}. Assuming that the sensitivity of our apparatus is similar to theirs, it follows that less than 7% of the area of the 7.237 keV resonance is due to the prompt capture of scattered neutrons. Although we expect that the prompt neutron sensitivity of our apparatus to be about the same as that of the similar setup at Geel, we do not know if this is the case. Therefore, we assign a rather large uncertainty to the area for the 7.237 keV resonance.

The average resonance properties, assuming that all the spin assignments in Tables III and IV are correct, are given in Table V. To maintain consistency with previous work [25], the *p*-wave strength functions were calculated using a radius of $1.35A^{1/3}$ fm.

Our ^{134,136}Ba(n,γ) cross sections for the unresolved resonance region are shown in Fig. 4. The data have been binned over the same coarse intervals used in previous work [9] for energies below 225 keV and in 25 keV wide bins for energies up to 500 keV.

The astrophysical reactivities $N_A\langle \sigma v \rangle$ calculated from our data are shown in Figs. 5 and 6 . The Maxwellian-averaged cross sections $\langle \sigma \rangle = N_A \langle \sigma v \rangle / N_A v_T$ calculated from our data at selected temperatures are given in Table VI. We show reactivities rather than average cross sections to better reveal the temperature dependence apart from the $1/v$ factor. The reactivities were calculated using our fits to the data below 11 keV in ^{134}Ba and 35 keV in ^{136}Ba and our cross section data above these energies. The statistical uncertainties in the reactivities are negligible compared to the overall normalization uncertainty. From the uncertainty in the ^{197}Au(n,γ) and ^{6}Li$(n,\alpha)\,^{3}$H cross sections [28], the statistical precision of the calibration measurements, and the repeatability of the calibration runs, we calculate that the normalization uncertainty is 3%.

IV. COMPARISON TO PREVIOUS WORK

Our data are compared to previous work in Figs. 4, 5, 6, 7, 8, and 9 and Table V. Our results represent a significant improvement over previous knowledge.

A. Resonance parameters and average cross sections

There have been two previous transmission measurements [29,30] from which resonance parameters were ascertained for ^{134}Ba and ^{136}Ba. These previous measurements were made with relatively poor resolution and sensitivity over a very restricted energy range, and so there is little overlap with our data. For the few resonances for which neutron widths were obtained in the previous works (seven in ^{134}Ba and three in ^{136}Ba), there is, in general, agreement with our data within the experimental uncertainties. The exceptions are that we did not observe the resonance in ^{134}Ba reported at 263 eV in Ref. [30], the width of the 1.616 keV resonance in ^{134}Ba reported in Ref. [29] is approximately 4 times larger than the value we obtained, and the width of the 1.885 keV resonance in ^{134}Ba reported in Ref. [30] is about 4 times smaller than the value we measured.

There have been one reported measurement [10] of the ^{134}Ba(n,γ) cross section from which resonance parameters were determined and two for ^{136}Ba [9,10]. Because there is a systematic difference between the results of Ref. [10] for ^{134}Ba compared to our results as well as those of Ref. [9], we will restrict the discussion to ^{136}Ba. The availability of resonance parameters obtained from three independent experiments offers the opportunity to examine the relative impor-

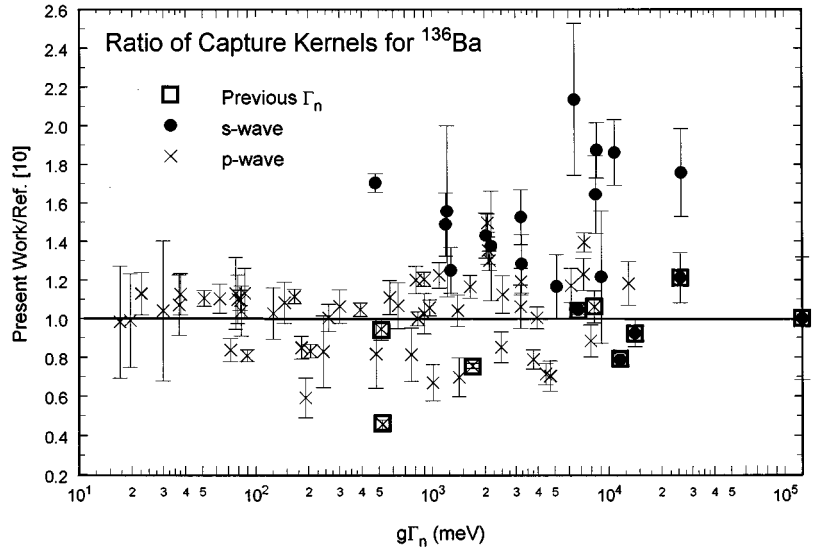

FIG. 7. Ratio of the capture kernels from the SAMMY fits to our data for ^{136}Ba to those of Ref. [10], versus the $g\Gamma_n$ values determined from the fits to our data. Data for resonances assigned as $l=0$ in Table IV are shown as solid circles whereas $l=1$ resonances are depicted as ×'s. Symbols surrounded by squares denote resonances for which estimates of the neutron widths were given in Ref. [10]. The error bars were calculated from the statistical uncertainties only.

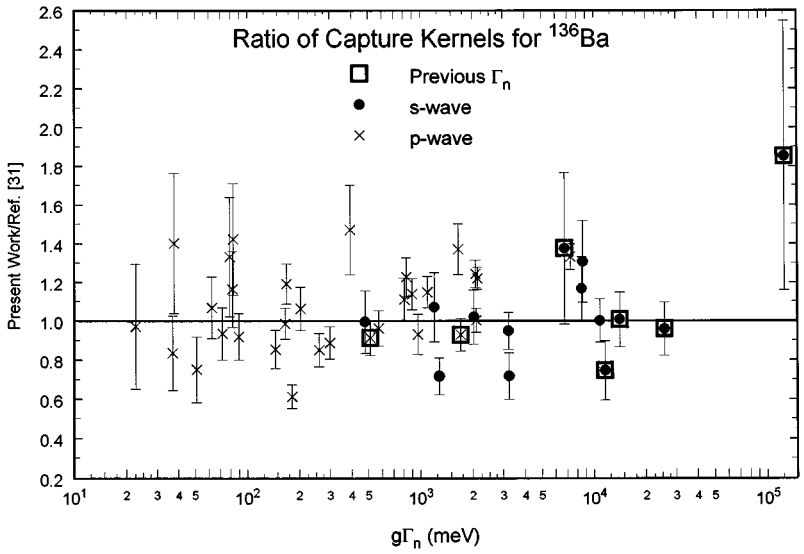

FIG. 8. Ratio of the capture kernels from the SAMMY fits to our data for ^{136}Ba to those of Ref. [31], versus the $g\Gamma_n$ values determined from the fits to our data. See the caption of Fig. 7 for details.

tance of the various correction factors applied to the data and to evaluate how well these corrections have been applied.

In Ref. [10], the neutron widths of a few resonances, the capture kernels for many resonances, and some average resonance parameters were reported over much of the same energy range as covered by our data. Several conclusions can be drawn from a comparison of our resonance parameters to those of Ref. [10]. For example, for the few resonances for which they were determined, the neutron widths in Ref. [10] are systematically larger than our values. More importantly, as can be seen in Fig. 7, the average ratio of capture kernels between the two experiments is close to 1, but more of the ratios are inconsistent with this average than expected from statistical considerations. Many of these deviations can probably be ascribed to the fact that $g\Gamma_n$ was not very well constrained by the measurements of Ref. [10]; hence, the wrong neutron widths apparently were used for many resonances in that work. Ascribing the deviations to the use of incorrect neutron widths is supported, for example, by the fact that the agreement between the two sets of capture kernels is fairly good for resonances which our measurements indicate have relatively small $g\Gamma_n$ values, but becomes worse for resonances with larger $g\Gamma_n$. Increasing deviations from the true capture kernels for larger $g\Gamma_n$ are expected when $g\Gamma_n$ is not well constrained because the corrections to the capture kernels due to finite-thickness sample effects increase with increasing $g\Gamma_n/\Gamma$. The fact that there is better agreement between the two sets of capture kernels for those few resonances for which the $g\Gamma_n$ values that were determined in Ref. [10] are close to our values also supports the contention that the nonstatistical deviations seen in Fig. 7 are due to the use of the wrong neutron widths in Ref. [10]. An alternative explanation, that the systematic difference between *s*- and *p*-wave resonances seen in Fig. 7 is due to the use of incorrect pulse height weighting functions, is ruled out by these same resonances. Unfortunately, the partial widths used to fit most of the resonances are not given in Ref. [10], and so it is not possible to explore this more fully.

Resonance parameters from a more recent measurement of the ^{136}Ba(n,γ) cross section were reported in Ref. [31]. These data were taken with a 4π BaF_2 detector, and so, in principle, a comparison between these data and ours could allow us to check our weighting functions as well as the neutron sensitivity of our apparatus. Ratios of our capture

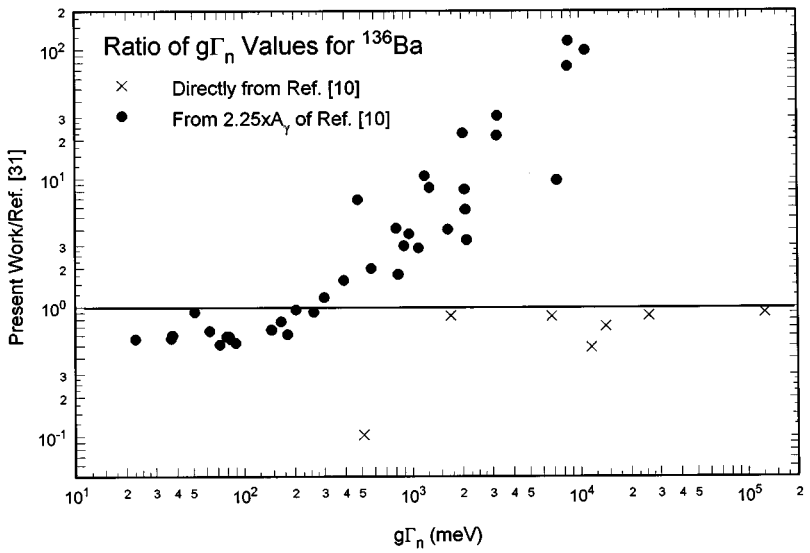

FIG. 9. Ratios of the $g\Gamma_n$ values determined from the fits to our data for ^{136}Ba to those used in Ref. [31] versus our $g\Gamma_n$ values. For most of the resonances (solid circles), it was assumed in Ref. [31] that $g\Gamma_n$ was restricted to the range of 1.5 – 3.0 times the capture kernel A_γ given in Ref. [10]. For this figure, we have chosen the midpoint of this range. For a few resonances ($\times$'s), the authors of Ref. [31] used the $g\Gamma_n$ values determined in Ref. [10].

kernels to those of Ref. [31] versus our $g\Gamma_n$ values are shown in Fig. 8. The average ratio in Fig. 8 is close to 1.0 but the fluctuations are larger than expected from the statistical uncertainties. The fluctuations are reduced somewhat if the resonances unresolved in Ref. [31] are combined, but still 17 of the 34 remaining ratios are inconsistent with an average ratio of 1.0. From this figure, it is evident that there is no trend in the ratios with $g\Gamma_n$ nor with the l value, indicating that the neutron sensitivity of our apparatus is small and that our pulse height weighting functions are correct. On the other hand, the fact that our value for the capture kernel for the 7.237 keV resonance is almost twice as large as the value in Ref. [31] appears to indicate that the 7% prompt neutron sensitivity correction we estimated for this resonance above, based on an apparatus similar to ours at Geel, is too small. However, the correction factor for this effect implied by the difference between our data and those of Ref. [31] for this resonance is so large (about 13 times larger than the correction factor estimated from the Geel experiment [27]) that significant corrections would be needed for several other resonances in ^{136}Ba. Using this larger correction factor worsens the agreement between our capture kernels and those of Ref. [31] for these resonances. For this reason, and because there is good agreement between our data and those of Ref. [10] for the 7.237 keV resonance, it seems likely that the capture kernel determined in Ref. [31] is too small.

The lack of any systematic trend in the ratio of capture kernels is encouraging, but it may be fortuitous. Because of the relatively poor resolution of the measurement, and because high-resolution transmission data were not available, the authors of Ref. [31] had to make some assumptions regarding the $g\Gamma_n$ values of the resonances. They used the $g\Gamma_n$ values from Ref. [10] for the few resonances for which they were assigned. For most resonances, however, they assumed that $g\Gamma_n$ was between 1.5 and 3.0 times the capture kernel for the resonance given in Ref. [10] and then Γ_γ was varied in the fit to the data. By using a range of $g\Gamma_n$ values they could estimate the uncertainty in the capture kernel associated with uncertainties in the self-shielding and multiple scattering corrections caused by changes in $g\Gamma_n$. The main problem with this approach, as can be seen in Fig. 9, is that the actual variations in $g\Gamma_n$ are much larger than the restricted range they considered. The result is that the self-shielding correction has apparently been underestimated for many of the resonances in Ref. [31]. As an indication of the impact that the size of the $g\Gamma_n$ value has on the self-shielding correction, in Ref. [31] it was stated that when the 4.702 keV resonance is analyzed using a $g\Gamma_n$ value of 1.5–3.0 times the capture kernel from Ref. [10], the resulting capture kernel is only 73% as large as the value obtained using the $g\Gamma_n$ value given in Ref. [10].

It is possible to correct the capture kernels of Ref. [31] using our $g\Gamma_n$ values. We calculated approximate correction factors by using an option in SAMMY to output the theoretical capture cross sections, both before (the ''true'' cross section) and after (the ''measured'' cross section) correction for resonance self-shielding. The self-shielding correction is given by the ratio of the ''measured'' to the ''true'' cross section. Two calculations were done using the sample thickness of Ref. [31], one with the resonances parameters of Ref. [31] and the other using our parameters. We used the median value for $g\Gamma_n$ in Ref. [31], 2.25 times the capture kernel from Ref [10], except for those resonances where $g\Gamma_n$ was taken directly from Ref. [10]. The Γ_γ values for Ref. [31] were then calculated using these neutron widths and the capture kernels of Ref. [31]. We then corrected the capture kernels of Ref. [31] by multiplying them by the ratio of the ''measured'' to ''true'' cross sections from the calculation with the parameters of Ref. [31] and dividing by the ratio from the calculation with our parameters. The overall agreement between the capture kernels from the two experiments was improved slightly by applying this correction. More significantly, because the neutron widths were most often underestimated in Ref. [31], most capture kernels were increased (by as much as 48%) by this correction. The overall effect of this correction is to increase the Maxwellian-averaged cross section calculated from the parameters of Ref. [31]. This will be discussed in the next subsection.

Finally, we note that from our transmission measurements alone, the capture kernel for the 4.948 keV resonance given in Ref. [31] is very likely too large. The capture kernel given in Ref. [31] is larger than the limit allowed by the most likely $g\Gamma_n$ value from the fit to our transmission data. Even if the largest $g\Gamma_n$ value allowed by our statistical uncertainty is used, the capture kernel in Ref. [31] would require an unreasonably large Γ_γ of 1120 meV.

The average resonance properties calculated from our parameters are compared to previous results [10,25] in Table V. Our results represent a significant improvement over previous knowledge. For example, there was very little previous information concerning the average p-wave properties and some previous s-wave averages were apparently contaminated by the inclusion of p-wave resonances. The average s-wave radiative widths $\langle\Gamma_{\gamma 0}\rangle$ we determined are substantially smaller than given in previous work. On the other hand, we were able to more precisely validate the assertion in Ref. [10] that the average p-wave radiative width of resonances in ^{136}Ba is substantially larger than that for s waves. Our values for the average level spacings are in agreement with previous work if the values given in Ref. [25] and the value for ^{134}Ba in Ref. [10] are assumed to include both s and p waves. The s-wave strength function for ^{136} Ba we calculate is in agreement with Ref. [25] whereas both our s- and p-wave strength functions for ^{134}Ba are substantially larger than given in Refs. [10,25]. ''Staircase'' plots of our s- and p-wave resonance data follow the expected linear behavior, lending confidence that the average resonance properties we calculate do not suffer significantly from systematic errors due to missing or misassigned levels.

Our measured cross sections for the unresolved resonance region are compared to previous work [9] in Fig. 4. Our data have been binned over the same course energy intervals used in Ref. [9] for energies below 225 keV. In general, there is fairly good agreement between the two sets of data for each nuclide.

B. Reaction rates

The astrophysical reactivities $N_A\langle\sigma v\rangle$ calculated from our measurements are compared to previous work [9,10,31] in Figs. 5 and 6. At the classical s-process temperature $kT=30$ keV, there is good agreement between our data and

the two previous measurements for ^{136}Ba [9,10], whereas for ^{134}Ba our data are in good agreement with the most recent measurement [9], confirming that the previous reaction rate of Ref. [10] is 20% too large.

Although there is good agreement with previous work at the classical *s* -process temperature, there are significant differences at other temperatures for both isotopes. In particular, near the lower temperatures ($kT \approx 8$ keV) favored by recent stellar models [1–3], our reaction rates for ^{134}Ba and ^{136}Ba are lower and higher, respectively, than in the previous work of Ref. [9]. The differences appear to be the effect of resonances below the energy range of the previous experiment. In Ref. [9], the contribution to the reaction rate due to resonances below 5 keV was estimated using calculations, whereas we directly measured the strengths of these resonances.

The lowest temperature for which reaction rates are available from previous work is 10 keV. For ^{134}Ba, our rate is only 89% as large as the rate in Ref. [9], where the contribution of resonances below 5 keV to the reaction rate at 10 keV was estimated to be 68.7 ± 6.9 mb [14], whereas our data show that they actually contribute only 47.0 mb. If the rate of Ref. [9] is corrected downward by this 21.7 mb difference, then the two rates agree to within the original experimental uncertainties.

For ^{136}Ba, our reaction rate at 10 keV is 6.2% higher than the rate reported in Ref. [9], where it was estimated [14] that resonances below 5 keV contribute 25.70 ± 5.14 mb to this rate, whereas our measurements show that they actually contribute 34.7 mb. If the rate of Ref. [9] is corrected upward by the difference between these two numbers, then the two rates agree to better than 2%.

Our reaction rate at $kT = 10$ keV is 11.2% larger than the rate determined from the resonance analysis of some of the ^{136}Ba(n,γ) data of Ref. [9] reported in Ref. [31]. However, if the contribution of resonances below the 2.8 keV cutoff of Ref. [31] and the effect of using incorrect neutron widths in Ref. [31] are taken into account, then there is very good agreement between our rate and theirs. Our data indicate that the resonances below 2.8 keV contribute 9.9 mb to the reaction rate at 10 keV. Our calculations described in the last subsection indicate that if the correct neutron widths are used, the 10 keV reaction rate is increased by another 3.6 mb over the value given in Ref. [31] . When these two effects are taken into account, the corrected rate of Ref. [31] is within 1% of our rate. The effect of resonances below the cutoffs of Refs. [9,31] on the reaction rate at other temperatures can be calculated using the parameters given in Tables III and IV. Our calculations indicate that if the reaction rates of Ref. [31] are corrected for the effect of using the wrong neutron widths, the rates at $kT = 20$ and 30 keV are increased by 2.0 and 1.1 mb, respectively.

Our measurements clearly demonstrate that ''...cross section measurements at low energies are urgently needed...'' as was stated in Ref. [9]. We have shown that resonances below the energy limit of previous experiments contribute substantially to the reaction rate at the low temperatures favored by recent stellar models and, furthermore, that the uncertainty associated with estimating the size of their contribution has been significantly underestimated in previous work [9,31]. Furthermore, we have shown that high-quality transmission measurements are indispensable for obtaining the correct reaction rates from resonance analyses.

V. ASTROPHYSICAL IMPLICATIONS

In Ref. [2], it was concluded that the isotopic anomalies of the barium isotopes observed in certain inclusions in meteorites could be reconciled with the predictions of models for the *s* process in low-mass stars only if the neutron capture reaction rates for the barium isotopes were adjusted from their then recommended values [32,33]. In Ref. [9] new measurements of these rates were reported that were closer to the adjusted values of Ref. [2] than the previously recommended values. However, even with these new cross sections, it was reported [9] that both classical *s*-process calculations as well as those based on a stellar model resulted in an overproduction of the *s*-only barium isotopes. As a result, it was suggested [9] that the solar barium abundance might be in error by 20%. Our new measurements of the reaction rates for ^{134}Ba and ^{136}Ba are significantly different from those of Ref. [9] at the low temperatures characteristic of the recent stellar models; hence, we have done some preliminary calculations to explore the effect of our new rates on the nucleosynthesis of the barium isotopes.

Because there is good agreement between our reaction rate and those of Ref. [9] at $kT = 30$ keV, there is no change in the barium abundances from classical *s*-process calculations. However, our data show that the ratio of reaction rates for the two *s*-only barium isotopes, which can be useful in estimating the *s*-process temperature, is a much stronger function of temperature than previously thought. The relatively strong decrease in the ^{134}Ba/^{136}Ba ratio of reaction rates indicated by our data has the effect of decreasing the effective *s*-process temperature from an analysis of the branching at ^{134}Cs compared to an analysis based on the reaction rates of Refs. [9,31]. Following Ref. [9], we used the classical approach to compute the *s*-process temperature by comparing the branching factor calculated from the neutron capture and β-decay rates of ^{134}Cs to the effective branching factor computed from the *s*-only barium isotopes. The results are illustrated in Fig. 10. The branching factor from the ^{134}Cs properties is given by

$$f_n = \lambda_n / (\lambda_n + \lambda_\beta), \tag{1}$$

where $\lambda_\beta = \ln 2 / t_{1/2}$ and $\lambda_n = n_n \sigma v_T$ [where n_n is the *s*-process neutron density, σ is the stellar ^{134}Cs(n,γ) cross section, and v_T is the mean thermal neutron velocity] are the β-decay and the neutron capture rates, respectively, for ^{134}Cs. The ^{134}Cs(n,γ) cross section was taken from Ref. [33] and was assumed to have a $1/v$ temperature dependence. The temperature dependence of the ^{134}Cs β-decay rate was taken from Ref. [34] and the neutron density $n_n = (4.1 \pm 0.6) \times 10^8$ cm^{-3} was taken from Ref. [35]. The temperature dependence of this branching factor is illustrated by the long-dashed, dotted, and dash-dotted curves in Fig. 10. The long-dashed curve depicts the temperature dependence of this branching factor using the recommended neutron capture and β-decay rates. The dotted curves show the uncertainty in this branching factor due to the uncertainty in

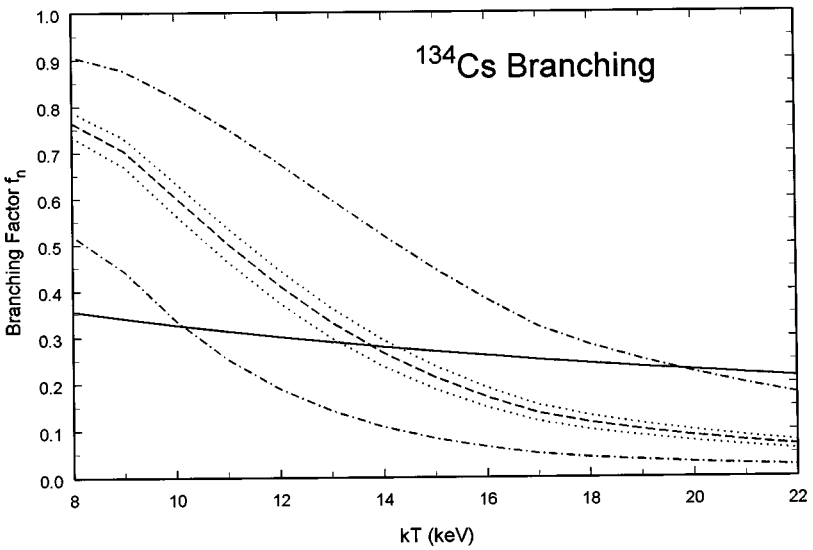

FIG. 10. The effective branching factor f_n at ^{134}Cs calculated under classical *s*-process assumptions. The long dashed curve shows the branching factor calculated from the ratio of the neutron and β-decay rates for ^{134}Cs [Eq. (1)] using the β-decay rate and neutron capture cross section recommended in Refs. [34] and [33], respectively. The two dotted curves show the uncertainty in the branching factor due to the uncertainty in the mean *s*-process neutron density. Similarly, the two dash-dotted curves depict the uncertainty in the branching factor due to a factor of 3 uncertainty in the temperature dependence of the β-decay rate for ^{134}Cs. The solid curve represents the branching factor calculated from the *s*-only barium isotopes [Eq. (2)] using our new ^{134,136}Ba(n,γ) reaction rates. The intersection of the solid curve with the long dashed curve yields the mean *s*-process temperature $kT \approx 14$ keV using the recommended parameters for ^{134}Cs. Similarly, the intersections of the solid curve with the dotted curves and the dash-dotted curves yield the range of temperatures allowed by the uncertainties in the *s*-process neutron density ($\pm$ 0.6 keV) and the temperature dependence of the ^{134}Cs β-decay rate ($+6$, -4 keV), respectively.

the neutron density whereas the dash-dotted curves depict the uncertainty due to the estimated factor of 3 uncertainty in the temperature dependence of the ^{134}Cs β-decay rate.

The effective branching factor from the *s*-only barium isotopes can be calculated from

$$f_n = 1 - \frac{\varsigma_{^{135}\mathrm{Ba}}\varsigma_{^{136}\mathrm{Ba}}(\sigma N_s)_{^{134}\mathrm{Ba}}}{(\sigma N_s)_{^{136}\mathrm{Ba}}}, \tag{2}$$

with

$$\varsigma_A = \left(1 + \frac{1}{\sigma_A \tau_0}\right)^{-1}. \tag{3}$$

The abundances N_s in Eq. (2) were taken from Ref. [36] and the mean exposure $\tau_0 = 0.295$ mb^{-1} was taken from Ref. [1]. The solid curve in Fig. 10 shows the temperature dependence of this branching factor using our reaction rates.

The effective, classical *s*-process temperature is given by the point where the curves for the two effective branching factors intersect. From the curves in Fig. 10 it can be seen that this occurs at $kT_s \approx 14$ keV. For comparison, a branching factor $f_n = 0.176$, independent of temperature, was calculated in Ref. [9], from which (using a smaller neutron density of 3.8×10^8 cm^{-3}) a higher temperature of $kT_s \approx 16$ keV was deduced. Allowing for a factor of 3 uncertainty in the ^{134}Cs β-decay rate, using our ^{134,136}Ba(n,γ) reaction rates results in a mean *s*-process temperature in the range $kT_s = 10$–20 keV. This is inconsistent with the value $kT_s = 29\pm5$ keV deduced from the analysis of the branchings at ^{151}Sm, ^{154}Eu, and ^{175}Lu [1]. This inconsistency in the temperature deduced from the classical analysis of different branching points apparently indicates a failure of the classical *s*-process scenario and points to the need for more sophisticated stellar models.

To investigate the nucleosynthesis in a more realistic model, we used the reaction network code NETZ [37] to calculate the *s*-process nucleosynthesis in a scenario approximating the recent stellar model of Ref. [2]. In this model of a low-mass red giant star, the main neutron exposure arises from the ^{13}C$(\alpha$,n) reaction at a temperature of $kT \approx 12$ keV. This is followed by a smaller exposure at $kT \approx 26$ keV due to the ^{22}Ne(α,n) reaction. Using NETZ, the neutron capture and β-decay connecting a series of 414 isotopes (including some isomers) between ^{28}Si and ^{211}Po was calculated over the course of 20 identical ''pulses.'' The time dependence of the temperature, neutron density, and electron density during each pulse approximated that from the stellar model. We performed two calculations, one with the reaction rates for ^{134,136}Ba from Ref. [9] and the second using our new rates. Reaction rates for the other isotopes were taken from Ref. [33] or from recent measurements reported since the time of that compilation.

Using the reaction rates of Ref. [31], the production of ^{134}Ba and ^{136}Ba is too high by 33% and 22%, respectively, normalized to the average overproduction of the *s*-only calibration points ^{124}Te and ^{150}Sm. Using our new reaction rates, the relative overproduction of ^{136}Ba compared to ^{124}Te and ^{150}Sm is decreased to 19% whereas the overproduction of ^{134}Ba is increased to 38%. Hence, the relative overproduction of the *s*-only barium isotopes remains a problem for this model.

In the more recent *s*-process model of Ref. [3], the neutron sources are the same, but ^{13}C(α,n) burns at a lower

temperature of $kT \approx 8$ keV between thermal pulses in a radiative rather than a convective environment. In addition, the neutron density during the $^{13}C(\alpha,n)$ phase is substantially smaller than in the 12 keV model [2]. However, the duration of this phase is longer so that the total number of neutrons released is about the same. Also, because the neutrons are released in a radiative rather than a convective environment, there is a range of conditions under which nucleosynthesis occurs depending on the distribution of primary ^{13}C and ^{14}N. Unfortunately, because of these and other differences compared to the 12 keV model, the current version of NETZ cannot be used to calculate the nucleosynthesis in this model in order to ascertain the effect of our new reaction rates. We can, however, make some general observations based on the temperature dependence of our reaction rates compared to those of Ref. [9].

The calculations of Ref. [3] show a relative overproduction of the *s*-only barium isotopes similar to that in the 12 keV model. Given the difference between our rates and those of Ref. [9] extrapolated to 8 keV, we expect that our new rates would reduce the overproduction of ^{136} Ba and increase the overproduction of ^{134}Ba in this model. However, there have been very few cross section measurements down to the low energies necessary to obtain accurate reaction rates at the low temperature of this model. Our measurements as well as similar data on ^{138}Ba [6] have shown that extrapolations from measurements at higher energies are not reliable; hence, new measurements are needed on many isotopes to fully evaluate this new model.

It might be possible to remedy the relative overproduction of ^{134}Ba by increasing the (n,γ) cross section and decreasing the β-decay rate of the radioactive branching point ^{134}Cs within the respective estimated uncertainties. However, our new lower $^{134}Ba(n,\gamma)$ reaction rate will make this more difficult. Also, the much lower neutron density in the 8 keV model could result in an even larger overproduction of ^{134}Ba. The lower neutron density is somewhat compensated by the fact that the β-decay lifetime of ^{134}Cs is substantially longer at the lower temperature. However, the fact that unbranched isotope ^{136}Ba is substantiallly overproduced in the model calculations indicates that there may be more fundamental problems with the stellar models and/or the solar barium abundance which should be addressed before ''fine-tuning'' is undertaken in an attempt to solve the ^{134}Ba overproduction.

VI. CONCLUSIONS

In conclusion, our measurements have allowed us to directly determine the rates for the $^{134,136}Ba(n,\gamma)$ reactions at the lower temperatures required by the new stellar models. Also, because our capture samples were thinner than those in previous measurements, and because we measured total as well as capture cross sections, we were able to substantially reduce systematic uncertainties associated with finite-thickness sample corrections to the data. We have shown that previous estimates for these low-temperature rates, based on extrapolations from higher-energy measurements, were substantially in error and that the ratio of reaction rates for these two isotopes depends more strongly on temperature than previously thought. Our analysis of the branching at ^{134}Cs using a classical *s* process scenario yielded a temperature too low to be consistent with the temperature from the analysis of other branching points. This inconsistency points to the need for more sophisticated models of the *s* process beyond the classical model. We have carried out *s*-process network calculations to explore the effect of our new reaction rates on the production of the barium isotopes in low-mass stars on the asymptotic giant branch. The calculations indicate that our new rates result in a reduction for ^{136}Ba, but an increase for ^{134}Ba, in their relative overproduction compared to other *s*-only isotopes. The relative overproduction of ^{134}Ba might be solved by adjusting the capture and β-decay rates for ^{134}Cs within their present uncertainties. However, the relative overproduction of the unbranched, *s*-only isotope ^{136}Ba remains a challenge to modelers of the *s* process.

ACKNOWLEDGMENTS

We are indebted to our colleagues at Oak Ridge National Laboratory and elsewhere who have contributed to the success of this work. In particular, we would like to thank F. Käppeler and K. Wisshak of Forschungszentrum Karlsruhe for graciously loaning us the material for the ^{134}Ba sample used in these measurements. We would also like to thank J.H. Hackney of the Analytical Chemistry Division for converting the nitrate portion of the sample into carbonate. We would like to express our appreciation to T.A. Lewis for keeping ORELA running smoothly, and to D.C. Larson and S. Raman for their help in attending the ORELA accelerator during the experiment. We would like to thank S. Jaag for valuable assistance in using the NETZ code. Finally, we would like to acknowledge helpful discussions with F. Käppeler, S. Jaag, and R. Gallino. This research was sponsored by the Oak Ridge National Laboratory which is managed by Lockheed Martin Energy Research Corporation for the U.S. Department of Energy under Contract No. DE-AC05-960R22464.

[1] F. Käppeler, R. Gallino, M. Busso, G. Picchio, and C. M. Raiteri, Astrophys. J. **354**, 630 (1990).

[2] R. Gallino, C. M. Raiteri, and M. Busso, Astrophys. J. **410**, 400 (1993).

[3] O. Straniero, R. Gallino, M. Busso, A. Chieffi, R. Raiteri, M. Limongi, and M. Salaris, Astrophys. J. **440**, L85 (1995).

[4] W. Howard, G. Mathews, K. Takahashi, and R. Ward, Astrophys. J. **309**, 633 (1986).

[5] F. Käppeler, H. Beer, and K. Wisshak, Rep. Prog. Phys. **52**, 945 (1989).

[6] H. Beer, F. Corvi, and K. Athanassopulos, in *Capture Gamma-Ray Spectroscopy and Related Topics*, edited by J. Kern

(World Scientific, Singapore, 1994), p. 698.
[7] A. D. L. Musgrove, B. Allen, J. Boldeman, and R. Macklin, Nucl. Phys. **A252**, 301 (1975).
[8] A. D. L. Musgrove, B. Allen, and R. Macklin, Aust. J. Phys. **32**, 213 (1979).
[9] F. Voss, K. Wisshak, K. Guber, F. Käppeler, and G. Reffo, Phys. Rev. C **50**, 2582 (1994).
[10] A. D. L. Musgrove, B. Allen, J. Boldeman, and R. Macklin, Nucl. Phys. **A256**, 173 (1976).
[11] J. Holmes, S. Woosley, W. Fowler, and B. Zimmerman, At. Data Nucl. Data Tables **18**, 305 (1976).
[12] S. Woosley, W. Fowler, J. Holmes, and B. Zimmerman, At. Data Nucl. Data Tables **22**, 371 (1978).
[13] F. Käppeler, K. Toukan, M. Schumann, and A. Mengoni, Phys. Rev. C **53**, 1397 (1996).
[14] F. Voss, K. Wisshak, K. Guber, F. Käppeler, and G. Reffo, Technical Report No. KfK 5253, Kernforschungszentrum Karlsruhe, 1994 (unpublished).
[15] F. Corvi, A. Prevignano, and H. Liskien, Nucl. Instrum. Methods A **265**, 475 (1988).
[16] F. Perey, J. Johnson, T. Gabriel, R. Macklin, R. Winters, J. Todd, and N. Hill, in *Nuclear Data for Science and Technology*, edited by S. Igarasi (Saikon, Tokyo, 1988), p. 379.
[17] R. Spencer, N. Larson, J. Todd, and L. Weston, in *Proceedings of the International Conference On Nucl. Data for Science and Technology*, edited by J. Dickens (American Nuclear Society, La Grange Park, IL, 1994), p. 99.
[18] *Gmelins Handbuch der Anorganischen Chemie, Barium* (Verlag Chemie GmbH, Berlin, 1932), Vol. 30, pp. 305–306.
[19] R. Macklin, N. Hill, J. Harvey, and G. Tweed, Phys. Rev. C **48**, 1120 (1993).
[20] R. Macklin and B. Allen, Nucl. Instrum Methods **91**, 565 (1971).
[21] W. Nelson, H. Hirayama, and D. Rogers, Technical Report No. SLAC-265, Stanford Linear Accelerator Center, 1985 (unpublished).
[22] R. Macklin, J. Halperin, and R. Winters, Nucl. Instrum. Methods **164**, 213 (1979).
[23] F. Fröhner, Technical Report No. GA-8380, Gulf General Atomic, Inc., 1968 (unpublished).
[24] N. Larson, Technical Report No. ORNL/TM-9179/R2, Oak Ridge National Laboratory, 1989 (unpublished).
[25] S. Mughabghab, M. Divadeenam, and N. Holden, *Neutron Cross Sections* (Academic, New York, 1981), Vol. 1.
[26] F. Fröhner, Technical Report No. KFK 2145, Kernforschungszentrum Karlsruhe, 1977 (unpublished).
[27] F. Corvi, P. Mutti, K. Athanassopulos, and H. Beer, in *Nuclei in the Cosmos III, Third International Symposium on Nuclear Astrophysics*, edited by M. Busso, R. Gallino, and C. Raiteri (American Institute of Physics, New York, 1955), p. 165.
[28] H. Beer and R. L. Macklin, Phys. Rev. C **26**, 1404 (1982).
[29] R. Alves, S. D. Barros, P. Chevillon, J. Julien, J. Morgenstern, and C. Samour, Nucl. Phys. **A134**, 118 (1969).
[30] R. V. de Vyver and N. Pattenden, Nucl. Phys. **A177**, 393 (1971).
[31] F. Voss, K. Wisshak, and F. Käppeler, Phys. Rev. **52**, 1102 (1995).
[32] H. Beer, F. Voss, and R. Winters, Astrophys. J. Suppl. **80**, 403 (1992).
[33] Z. Bao and F. Käppeler, At. Data Nucl. Data Tables **36**, 411 (1987).
[34] K. Takahashi and K. Yokoi, At. Data Nucl. Data Tables **36**, 375 (1987).
[35] K. Toukan, K. Debus, and F. Käppeler, Phys. Rev. C **51**, 1540 (1995).
[36] E. Anders and N. Grevess, Geochim. Cosmochim. Acta **53**, 197 (1989).
[37] S. Jaag, Diploma thesis, University of Karlsruhe, 1991.